CORE
Metadata, citation and similar papers at core.ac.uk
Provided by Elsevier - Publisher Connector
Cell, Vol. 102, 89–97, July 7, 2000, Copyright ©2000 by Cell Press

Congenital Deafness and Sinoatrial Node Dysfunction in Mice Lacking Class D L-Type Ca^{2+} Channels

Josef Platzer,[1] Jutta Engel,[2] Anneliese Schrott-Fischer,[3] Kurt Stephan,[3] Sergio Bova,[4] Howard Chen,[5] Hui Zheng,[5,7] and Jörg Striessnig[1,6]

[1]Institut für Biochemische Pharmakologie
Peter-Mayrstr. 1
A-6020 Innsbruck
Austria

[2]Physiologisches Institut II/Sektion Sensorische Biophysik der HNO-Klinik
Universität Tübingen
Röntgenweg 11
D-72076 Tübingen
Germany

[3]Universitätsklinik für Hals-, Nasen- und Ohrenheilkunde
Anichstr. 25
A-6020 Innsbruck
Austria

[4]Dipartimento di Farmacologia
Universita Degli Studi Di Padova
Largo E. Meneghetti 2
I-35131 Padova
Italy

[5]Department of Metabolic Disorders
Merck Research Laboratories
Rahway, New Jersey 07065

Summary

Voltage-gated L-type Ca^{2+} channels (LTCCs) containing a pore-forming α1D subunit (D-LTCCs) are expressed in neurons and neuroendocrine cells. Their relative contribution to total L-type Ca^{2+} currents and their physiological role and significance as a drug target remain unknown. Therefore, we generated D-LTCC deficient mice (α1D$^{-/-}$) that were viable with no major disturbances of glucose metabolism. α1D$^{-/-}$ mice were deaf due to the complete absence of L-type currents in cochlear inner hair cells and degeneration of outer and inner hair cells. In wild-type controls, D-LTCC-mediated currents showed low activation thresholds and slow inactivation kinetics. Electrocardiogram recordings revealed sinoatrial node dysfunction (bradycardia and arrhythmia) in α1D$^{-/-}$ mice. We conclude that α1D can form LTCCs with negative activation thresholds essential for normal auditory function and control of cardiac pacemaker activity.

Introduction

Different types of voltage-gated Ca^{2+} channels mediate depolarization-induced Ca^{2+} influx across the plasma membrane of electrically excitable cells, thereby controlling key physiological processes. One class, L-type Ca^{2+} channels (LTCCs), are activated by strong depolarizations and are modulated by low concentrations of different chemical classes of Ca^{2+} antagonists, including dihydropyridines (DHPs; Striessnig, 1999). LTCCs are widely expressed in mammalian organisms. In skeletal, smooth, and cardiac muscle, they couple membrane depolarization to muscle contraction. In (neuro)endocrine cells, including pancreatic β cells, Ca^{2+} influx through LTCCs triggers hormone secretion (Ashcroft and Rorsman, 1989). In neurons, LTCCs are preferentially located at cell bodies and dendrites (Hell et al., 1993) and play only a minor role for neurotransmitter release at nerve terminals. Ca^{2+} influx through neuronal LTCCs into the cell soma modulates gene transcription, thus coupling synaptic excitation to transcriptional events thought to contribute to neuronal plasticity (Murphy et al., 1991; Deisseroth et al., 1998; Hardingham et al., 1998; Tao et al., 1998; Graef et al., 1999; Rajadhyaksha et al., 1999). Recently a retina-specific LTCC isoform has been discovered that is likely to control neurotransmitter release from photoreceptor presynaptic terminals (Bech-Hansen et al., 1998; Strom et al., 1998).

LTCCs form multisubunit complexes containing different isoforms of pore-forming α1 subunits, termed α1C, α1D, α1F, and α1S (Striessnig, 1999). LTCCs formed by α1C (C-LTCCs) represent the most abundant isoform in the cardiovascular system. It is therefore believed that the therapeutic effects of Ca^{2+} antagonist drugs are mainly mediated by block of C-LTCCs.

The differential contribution of LTCCs formed by α1C and α1D subunits (D-LTCCs) to total L-type Ca^{2+} current in mammalian tissues such as brain (Hell et al., 1993), heart atria (Takimoto et al., 1997), and pancreatic β cells (Iwashima et al., 1993) is unclear because both isoforms are expressed in these tissues. The same is true for the cochlea, where both isoforms have been detected by PCR (Green et al., 1996). A recent study revealed that hair cells of the chick basilar papilla predominantly express the α1D subunit (Kollmar et al., 1997), suggesting a role for class D-LTCCs for afferent synaptic transmission. In brain (Hell et al., 1993) and heart (Takimoto et al., 1997), α1D is much less abundant than α1C, suggesting that D-LTCCs may serve a discrete functional role. In contrast, α1D mRNA is more abundant in rat pancreatic islets and thus believed to be mainly responsible for stimulus–secretion coupling in pancreatic β cells (Iwashima et al., 1993).

D-LTCCs cannot be distinguished pharmacologically from C-LTCCs (Williams et al., 1992). Due to the absence of selective blockers, it has been impossible to assess their exact physiological role and potential significance as a selective drug target. We have therefore generated mice lacking the D-LTCC α1D subunit (α1D$^{-/-}$ mice, Figure 1) by homologous recombination in mouse embryonic stem cells. Here we report that α1D$^{-/-}$ mice are deaf and exhibit bradycardia and arrhythmia resulting from sinoatrial node dysfunction. Our experiments revealed that Ca^{2+} currents which couple sound-evoked depolarization in cochlear inner hair cells (IHCs) to neurotransmitter release are almost exclusively mediated by

[6]To whom correspondence should be addressed (e-mail: joerg.striessnig@uibk.ac.at).
[7]Present address: Huffington Center on Aging, Baylor College of Medicine, Houston, Texas 77030.

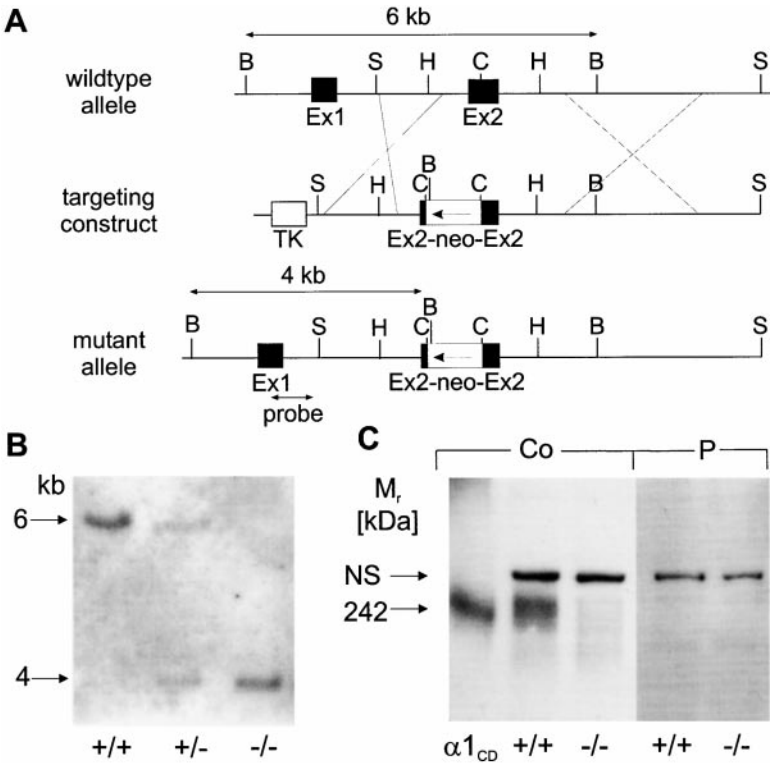

Figure 1. Targeted Mutagenesis and Expression Analysis of the α1D Ca^{2+} Channel Subunit

(A) Restriction enzyme map of the wild-type and mutant α1D subunit alleles and of the targeting construct. Exon 1 (Ex1) and exon 2 (Ex2) are indicated by black boxes. The neomycin resistance gene (*neo*) was inserted in reverse direction into the ClaI restriction site of exon 2 introducing also a BamHI site. The thymidine kinase gene (*TK*) was used to select against random integration. Homologous recombination was expected to yield an α1D subunit truncated before the first transmembrane segment (IS1). B, BamHI; S, SpeI; H, HindIII; C, ClaI.

(B) Verification of genotypes by Southern blot analysis of genomic DNA digested with BamHI from wild-type (+/+), heterozygous (+/−), and homozygous mutants (−/−) using the probe indicated in (A). The wild-type allele generates a 6 kb and the mutant allele a 4 kb band (arrows).

(C) Verification of α1D subunit deficiency by Western blot analysis of brain microsomal membrane protein using affinity-purified polyclonal antibody anti-$\alpha1D_{2121-2137}$. The migration of α1D immunoreactivity and of a recombinant α1C/α1D chimera containing the antibody epitope ($\alpha1_{CD}$, calculated molecular mass 242 kDa) is indicated (arrow). Specific α1D staining was absent after preincubation of antibody with the antigenic peptide (0.25 μM). NS indicates a nonspecific band recognized by the antibody. Co, control; P, antibody staining in the presence of antigenic peptide under otherwise identical experimental conditions. One of three experiments yielding the same result is shown.

D-LTCCs. In addition, D-LTCCs are required for normal cardiac pacemaking.

Results

The gene-targeting strategy is illustrated in Figure 1A. Successful gene targeting and the generation of a complete null allele was confirmed by Southern blot analysis of genomic DNA (Figure 1B) and Western blot analysis of mouse brain membrane protein using a polyclonal antibody against α1D, respectively (Figure 1C).

$\alpha1D^{-/-}$ mice displayed normal sexual activity and reproduction and exhibited no obvious anatomical abnormalities. Homozygous pups were slightly underrepresented in litters from heterozygous parents (wild type: 35%; heterozygous: 50%; homozygous: 15%; n = 180). However, no decrease in the number of pups was found in homozygous crossings. No differences in growth of $\alpha1D^{-/-}$ mice were found.

$\alpha1D^{-/-}$ mice reacted differently to auditory stimuli than their wild-type littermates. The Preyer reflex, a motor reflex in response to an auditory stimulus (Bohmer, 1988), could be elicited by hand claps in wild-type and heterozygous animals but was completely absent in all $\alpha1D^{-/-}$ mice (n > 50). Measurement of click-evoked auditory brainstem responses (ABRs) confirmed normal hearing thresholds (Zheng et al., 1999) in 5- to 8-week-old wild-type and heterozygous mice (30–40 dB SPL [sound pressure level], n > 9) but deafness in $\alpha1D^{-/-}$ littermates (hearing threshold, >120 dB SPL, n = 10) (Figure 2).

Voltage-gated Ca^{2+} channels couple membrane depolarization to neurotransmitter release in auditory hair cells (Martinez-Dunst et al., 1997; Moser and Beutner, 2000). Our mouse model enabled us to determine the relative contribution of D-LTCCs to whole-cell Ca^{2+} channel currents in IHCs in the semiintact organ of Corti by comparing Ca^{2+} current densities in wild-type and $\alpha1D^{-/-}$ mice using the whole-cell configuration of the patch-clamp technique (10 mM Ba^{2+} as charge carrier).

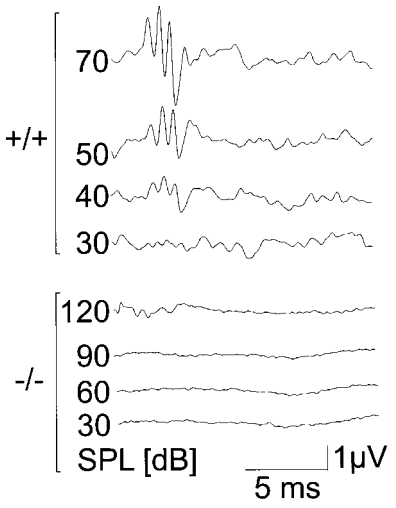

Figure 2. Effects of α1D Deficiency on Auditory Function

ABRs of 5-week-old wild-type (+/+) and $\alpha1D^{-/-}$ (−/−) mice. Representative experiments are shown. The typical ABR waveform was present above 30 dB SPL in wild type (+/+) but was absent in $\alpha1D^{-/-}$ mice. The waves at 120 dB SPL in $\alpha1D^{-/-}$ mice represent background because they were also observed in control experiments without animals and did not show the typical ABR waveform.

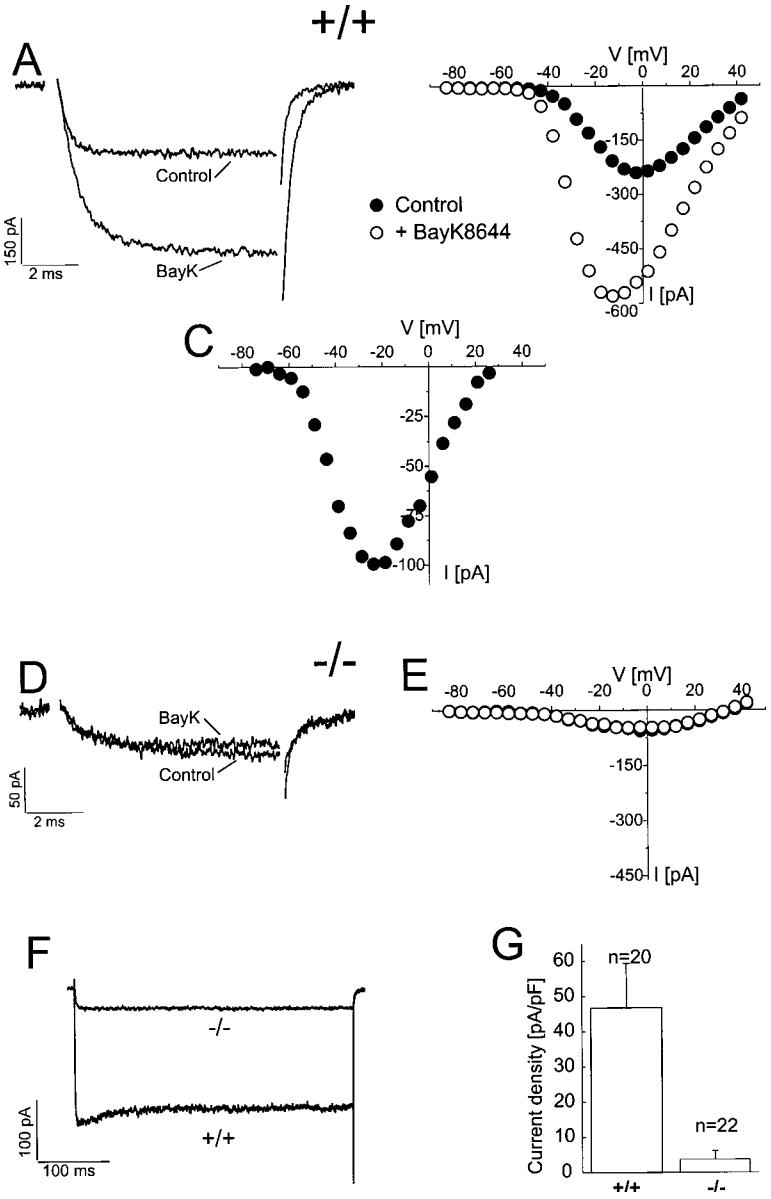

Figure 3. Ba^{2+} and Ca^{2+} Currents through LTCCs in IHCs

Current recordings in isolated IHCs were carried out as described in Experimental Procedures. Peak I_{Ba} current traces in IHCs isolated from 9-day-old $\alpha1D^{+/+}$ (A) and $\alpha1D^{-/-}$ mice (D) were elicited by 8 ms depolarizing steps from a holding potential of −83 mV to the potential of peak current (−2 mV, except −12 mV in [A], trace BAYK), in the absence (control) and 2 min after superfusion with the DHP Ca^{2+} channel activator BAYK8644 (BayK, 5 μM). Corresponding I-V curves (B and E) are also shown. (C) I-V curve recorded in a $\alpha1D^{+/+}$ IHC isolated from a 3-day-old mouse using 1.3 mM extracellular Ca^{2+} as the charge carrier. Note the negative activation threshold and peak. One representative experiment (of $n > 8$) is shown. (F) I_{Ba} in $\alpha1D^{+/+}$ (+/+) and $\alpha1D^{-/-}$ mice (−/−) during 400 ms depolarizations to −2 mV. (G) Mean current densities (±SD) for $\alpha1D^{+/+}$ (+/+) and $\alpha1D^{-/-}$ mice (−/−) obtained from the indicated number of cells.

The detailed properties of voltage-gated Ca^{2+} currents have not been characterized in mammalian hair cells so far. In IHCs isolated from wild-type mice aged from postnatal day 3 (P3) to P9, depolarizations from a holding potential of −83 mV to different test potentials between −83 and +53 mV elicited rapidly activating (τ_{act} = 0.31 ± 0.03 ms, n = 7) and slowly inactivating inward Ba^{2+} currents (I_{Ba}) through Ca^{2+} channels (11.1% ± 4.8% of peak current inactivated after 300 ms, n = 18) (Figures 3A and 3F). Slow inactivation was also observed when Ca^{2+} (10 mM) was the permeating ion (21.1% ± 9.3% after 300 ms, n = 5). Maximal I_{Ba} was elicited by depolarizations to −2.1 ± 2.7 mV (n = 20) (Figures 3A and 3B) with a half-maximal voltage of steady-state activation at −16.5 ± 2.6 mV (n = 20). L-type currents activated at relatively low voltages. Activation thresholds were −50 to −40 mV with 10 mM Ba^{2+} (Figure 3B) or 10 mM Ca^{2+} (data not shown) as charge carrier. With 1.3 mM Ca^{2+} as a charge carrier (physiological concentration), the current started activating as negative as −65 mV and peaked at −25 mV (Figure 3C). Ba^{2+} currents were increased to 292% ± 56% (n = 7) of control I_{Ba} by the DHP activator BAYK8644 (5 μM) and decreased to 59% ± 8% of control (n = 4) by the DHP channel blocker nimodipine (10 μM), confirming that at least part of I_{Ba} was carried by LTCCs (Figures 3A, 3B, 3D, and 3E). Our data show that LTCCs in mammalian IHCs exhibit the same unusual gating kinetics (i.e., more negative activation threshold, rapid activation, slow inactivation) as previously described for L-type Ca^{2+} currents in frog (Hudspeth and Lewis, 1988) and chick hair cells (Fuchs et al., 1990; Zidanic and Fuchs, 1995).

I-V curves, current kinetics, modulation by DHPs (data not shown), and maximal I_{Ba} densities were similar in wild-type (46.8 ± 12.6 pA/pF, n = 20) and heterozygous animals (51.9 ± 30.9 pA/pF, n = 10). However, current density was dramatically decreased in IHCs recorded from $\alpha1D^{-/-}$ mice (Figure 3). Currents obtained under identical experimental conditions were >90% smaller (3.7 ± 2.5 pA/pF, n = 22) and resistant to modulation

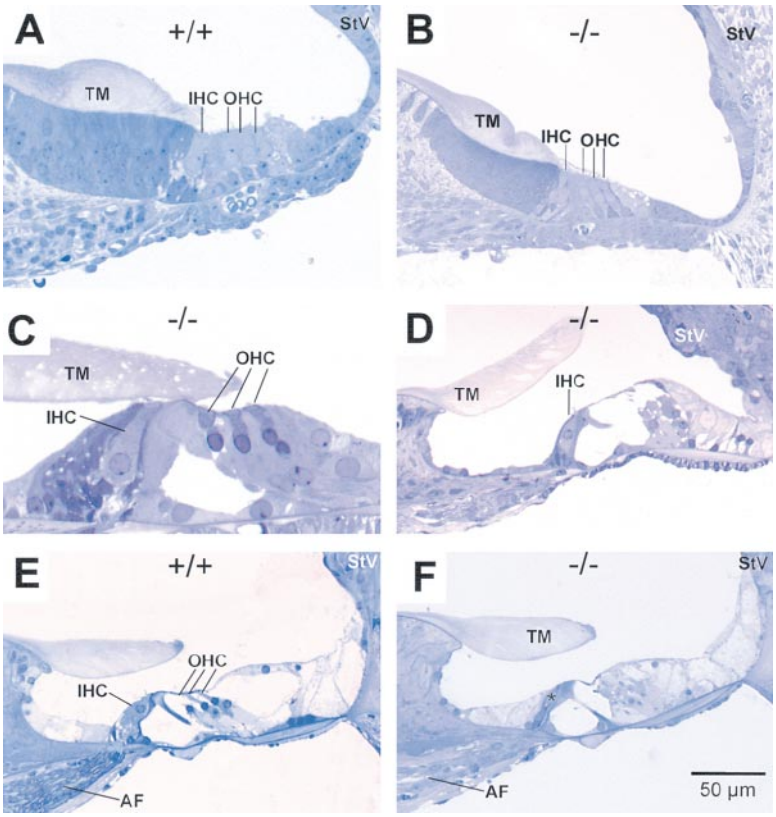

Figure 4. Effects of α1D Deficiency on Inner Ear Histology

(A and B) Two micrometer sections of mouse cochleae stained with toluidine blue are shown. Normal appearance of the organ of Corti in 3-day-old wild-type (+/+) (A) and $\alpha1D^{-/-}$ (−/−) (B) littermates.

(C) Normal histology in 7-day-old $\alpha1D^{-/-}$ mice.

(D) Pronounced degeneration of outer hair cells (OHCs) at P14 in $\alpha1D^{-/-}$. OHCs are absent with degeneration starting on the apical side. A normally appearing IHC is indicated.

(E) Normal histology in wild-type mice at P35.

(F) Complete degeneration of OHCs and IHCs at P35 in $\alpha1D^{-/-}$ mice. The asterisk indicates the absence of an inner hair cell and shows the presence of a remaining supporting cell visible in some sections. At this stage, the afferent neurons (AF) are clearly degenerated in $\alpha1D^{-/-}$ but appear normal in $\alpha1D^{+/+}$ mice. TM, tectorial membrane; StV, stria vascularis. A scale bar is shown for the section in (F).

by DHPs (Figures 3D–3G). Cell membrane capacitance, as a measure of cell size, was not altered by gene disruption (P1–P9: wild type, 6.3 ± 1.8 pF, n = 20; $\alpha1D^{-/-}$, 6.3 ± 0.9 pF, n = 22). Histological examination of 2 μm sections of mouse cochleae by light microscopy also did not reveal any morphological changes of IHCs and ganglion cells up to P14 in $\alpha1D^{-/-}$ mice (Figures 4B–4D), although complete deafness was already present at this age (hearing threshold: wild type, 50–60 dB SPL; $\alpha1D^{-/-}$, >120 dB, n = 4). Therefore, the reduction of inward current appears not to occur secondary to changes of IHC morphology. At P14, degeneration of outer hair cells (OHCs) was present in $\alpha1D^{-/-}$ but not wild-type mice (Figure 4D), and OHCs as well as IHCs were absent at P35, when degeneration of the afferent nerve fibers (Figures 4E and 4F) and ganglion cells (data not shown) was also observed.

As α1D mRNA is also expressed in atrial (but not ventricular) cardiomyocytes (Takimoto et al., 1997), we examined $\alpha1D^{-/-}$ mice for possible alterations in cardiac function. Electrocardiograms (ECGs) and physical activity were simultaneously recorded by telemetry in unrestrained conscious mice. The R wave is the prominent upward deflection of the QRS complex caused by excitation of the heart ventricles (indicated in Figures 5D and 5E). The R–R interval can therefore be used to quantitate heart rate (beats per minute = 60,000 divided by R–R interval in milliseconds) as well as arrhythmia (R–R variability). In all homozygous but none of the wild-type littermates, pronounced bradycardia (evident as an increased mean R–R interval) and arrhythmia (evident as a high standard deviation of R–R intervals) was present at rest (Figures 5A and 5B, I). A prolongation of the P–R interval as a measure of atrioventricular (AV) conduction velocity was also found (wild type: 43 ± 2 ms, n = 5; $\alpha1D^{-/-}$: 54 ± 3 ms, n = 6; $p < 0.01$). In addition, episodes of second degree AV block (7 out of 11 $\alpha1D^{-/-}$; 0 out of 8 $\alpha1D^{+/+}$) were recorded in knockout animals (Figure 5E). In wild-type and $\alpha1D^{-/-}$ mice, QRS complexes were triggered by normal P waves (Figures 5C–5E). Bradycardia and arrhythmia must therefore involve altered sinoatrial node pacemaker activity.

Bradycardia and arrhythmia were reduced during episodes of enhanced spontaneous physical activity (Figures 5A and 5B, II), indicating that the severity of this phenotype depends on autonomic tone. They were abolished after block of cardiac muscarinic receptors by atropine (1 mg/kg i.p.; Figures 5A and 5B, IV). If bradycardia would be caused only by altered autonomic tone alone without intrinsic disturbances in sinoatrial node pacemaker activity, then the difference between wild-type and $\alpha1D^{-/-}$ mice must disappear after pharmacological block of sympathetic and parasympathetic activation. Cardiac muscarinic and β-adrenergic receptors were blocked by combined i.p. injection of atropine (1 mg/kg) and propranolol (20 mg/kg) at concentrations known to abolish autonomic control of the heart (Jumrussirikul et al., 1998; Wickman et al., 1998). Figure 5 (III) illustrates that pronounced bradycardia and arrhythmia persisted even after this treatment. Similarly, if bradycardia was only due to increased parasympathetic tone (as suggested by the atropine experiments), then the difference should be diminished during strong parasympathetic activation in both wild-type and $\alpha1D^{-/-}$ mice. This was clearly not the case. Application of the α1-adrenergic agonist methoxamine induces bradycardia by causing vasoconstriction and elevation of blood pressure resulting in a reflex stimulation of vagal activity

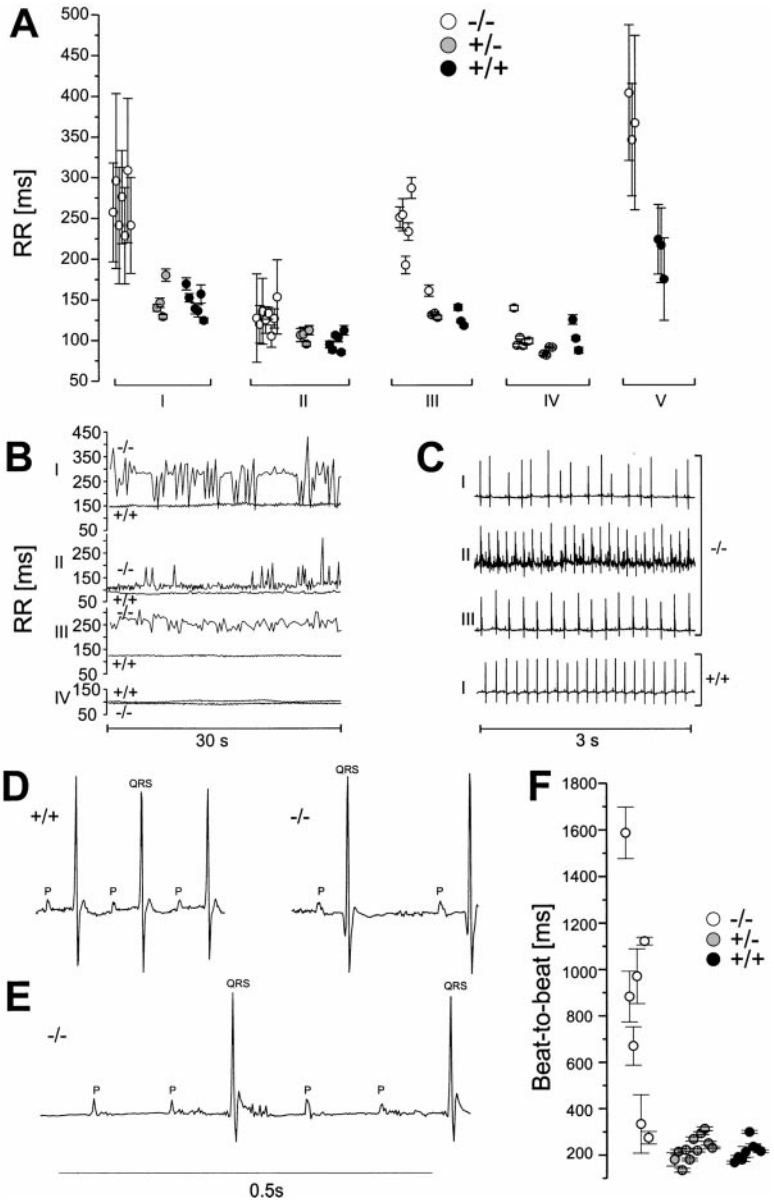

Figure 5. Sinoatrial Node Bradycardia and Arrythmia in $\alpha 1D^{-/-}$ Mice

(A) Mean R–R intervals from individual wild-type (+/+), heterozygous (+/−), and homozygous (−/−) mutant mice were calculated from 30 s episodes of telemetric ECG recordings during rest (I), spontaneous physical activity (II), 10 min after administration of atropine (1 mg/kg body weight i.p.) plus propranolol (20 mg/kg i.p.) (III), atropine alone (IV), and methoxamine (6 mg/kg i.p.) (V). Note that the standard deviation of R–R intervals is a measure of the extent of sinus arrhythmia. SD was smaller than the size of the symbols for most wild-type and heterozygous animals.

(B) Typical recordings of R–R intervals during 30 s intervals under the experimental conditions described in (A).

(C) Telemetric ECG waveforms obtained simultaneously from unrestrained mice during a 3 s interval.

(D) ECG waveforms (lead I, 0.25 s) recorded from wild-type (+/+) and $\alpha 1D^{-/-}$ mice (−/−). P waves and QRS complexes are indicated.

(E) Typical episode of second degree AV block in a $\alpha 1D^{-/-}$ mouse. Note that only every second P wave is followed by a QRS complex.

(F) Bradycardic and arrhythmic heart beat in spontaneously beating isolated heart atria. Mean beat to beat intervals (as a measure of heart rate) and the corresponding standard deviation (as a measure of arrhythmia) were calculated from 10 s recordings 60–75 min after the equilibration period in $\alpha 1D^{+/+}$, $\alpha 1D^{+/-}$, and $\alpha 1D^{-/-}$ mice.

and strong activation of muscarinic receptors controlling heart rate (Wickman et al., 1998). After methoxamine treatment (6 mg/kg i.p.), the difference in heart rate persisted as R–R intervals were increased both in $\alpha 1D^{-/-}$ and $\alpha 1D^{+/+}$ mice to similar extents (Figure 5, V). Thus, pharmacological block of autonomic control and methoxamine treatment are compatible with an intrinsic sinoatrial node dysfunction.

To obtain direct functional evidence for sinoatrial node dysfunction in $\alpha 1D^{-/-}$ mice, heart rate was measured in completely denervated, spontaneously beating isolated heart atria. Again, a much slower heart rate and/or more pronounced arrhythmia was found under these conditions for knockout mice as compared to heterozygous and wild-type animals (Figure 5F).

Taken together these findings demonstrate that the absence of D-LTCCs in mouse atria results in disturbed cardiac pacemaker activity in the absence of autonomic control or when parasympathetic tone predominates. Although our experiments do not rule out that altered autonomic control does also contribute to the heart rate disturbances to some extent in $\alpha 1D^{-/-}$ mice, $\alpha 1D$ gene knockout clearly demonstrated a role of D-LTCCs for sinoatrial node pacemaker activity.

No evidence for other disturbances of action potential generation and propagation was found: QRS complex duration ($\alpha 1D^{+/+}$: 14.8 ± 1.8 ms, n = 6; $\alpha 1D^{-/-}$: 15.7 ± 3.5 ms, n = 8) was not significantly different in knockout animals, indicating that myocardial action potential propagation was normal. Light microscopy revealed no anatomical abnormalities or changes in the myocardial architecture, myocyte shape and size, and sinoatrial node architecture (data not shown). Note that the absence of structural abnormalities is in accordance with the finding that pacemaker activity indistinguishable from wild type can be reestablished in $\alpha 1D^{-/-}$ mice after atropine treatment. Differences in heart rate could not be explained by alterations in plasma catecholamine

levels (plasma norepinephrine concentration: wild type, 11.8 ± 3.6 pg/ml; $\alpha1D^{-/-}$, 8.4 ± 2.1 pg/ml, mean ± SEM, n = 5). Auditory development as well as cardiac function could be due to abnormal thyroid hormone activity (Forrest et al., 1996; Johansson and Thoren, 1997). We found no difference in hormone levels that could account for our phenotype (hormone plasma concentrations—free T3: $\alpha1D^{+/+}$, 1.43 ± 0.17 pg/ml, $\alpha1D^{-/-}$, 1.13 ± 0.18 μg/ml; free T4: $\alpha1D^{+/+}$, 14.27 ± 1.70 pg/ml, $\alpha1D^{-/-}$, 13.04 ± 2.50 pg/ml, mean ± SEM, n > 7).

As D-LTCCs are believed to represent the major LTCC species responsible for stimulus–secretion coupling in pancreatic β cells (Iwashima et al., 1993; Yamada et al., 1995), we also measured serum glucose and insulin levels in fasting animals and after response to a glucose challenge. Decreased LTCC activity in these cells should lead to decreased insulin secretion and increased serum glucose concentrations. Fasting glucose levels ($\alpha1D^{+/+}$: 5.5 ± 0.4 mM; $\alpha1D^{-/-}$: 4.9 ± 0.2 mM, mean ± SEM, n > 7) were slightly but not significantly lower in $\alpha1D^{-/-}$ mice than in wild-type littermates. No difference in serum glucose levels was observed 30 min after i.p. application of 1.5 mg/g body weight of glucose ($\alpha1D^{+/+}$: 17.2 ± 1.1 mM; $\alpha1D^{-/-}$: 15.7 ± 1.4 mM, mean ± SEM, n > 7). Insulin levels were also not different in fasting mice ($\alpha1D^{+/+}$: 0.21 ± 0.06 ng/ml; $\alpha1D^{-/-}$: 0.25 ± 0.05 ng/ml, mean ± SEM, n > 7) and 30 min after the glucose challenge ($\alpha1D^{+/+}$: 0.51 ± 0.08 ng/ml; $\alpha1D^{-/-}$: 0.55 ± 0.07 ng/ml, mean ± SEM, n > 7). Therefore, insulin secretion in mice is not strictly dependent on D-LTCC expression in pancreatic β cells. We cannot exclude that this is due to a compensatory upregulation of C-LTTCs that are also abundant in these cells (Iwashima et al., 1993; Safayhi et al., 1997).

Discussion

Our analysis of the α1D gene knockout mice provides important new insight into the physiological function and pharmacotherapeutic potential of D-LTCCs. By measuring ABRs, we show that α1D deficiency results in congenital deafness. Hearing starts in mice between P10 and P12. Although we had no evidence for morphological changes of IHCs before P14, we found a >90% decrease in voltage-gated Ca^{2+} current. D-LTCCs comprised all L-type Ca^{2+} current and >90% of the total Ca^{2+} current in mammalian IHCs. Deafness can therefore be explained by an almost complete loss of Ca^{2+} influx that couples mechanically induced depolarization to neurotransmitter release at the IHC synapse (Moser and Beutner, 2000). OHCs, which show very little afferent innervation, are responsible for mechanical amplification of sound stimuli. Degeneration of OHCs (already evident at P14) alone would not cause deafness but could contribute to the elevation of the hearing threshold by 40–50 dB (Liberman and Dodds, 1984). Our pathohistological findings demonstrate that D-LTCCs are required to maintain normal cochlear morphology. Further studies are necessary to determine if the degeneration of OHCs results from abnormal IHC signaling alone or is due to the absence of D-LTCC in other cells (e.g., OHCs).

Our data also prove that the unusual electrophysiological L-type Ca^{2+} current properties (negative activation threshold, fast activation, slow inactivation of I_{Ba} and I_{Ca}) described here and in previous studies with chick basilar papilla hair cells (Zidanic and Fuchs, 1995) can be exclusively attributed to D-LTCCs in mice IHCs. Although both α1C and α1D transcripts have been detected in mouse cochlea (Green et al., 1996), we found no evidence for a second DHP-sensitive Ca^{2+} current component, excluding the presence of α1C-mediated currents in $\alpha1D^{-/-}$ mice. It is also interesting that the hearing loss was not associated with gross disturbances in vestibular function and structure up to P35 (data not shown). This suggests that α1D plays a less prominent role in the formation of voltage-gated Ca^{2+} channels found in mammalian type I and II vestibular hair cells (Boyer et al., 1998; Lopez et al., 1999).

No hearing impairment has been reported during therapy with Ca^{2+} channel blockers in humans, and high doses of DHPs do not increase hearing threshold in mice (Ison et al., 1997). Our experiments show that these findings are not due to the absence of DHP-sensitive Ca^{2+} current components in IHCs. Instead, this must be due to the relatively low DHP sensitivity of D-LTCCs at negative holding potentials determined in our experiments and in chick hair cells (Fuchs et al., 1990).

A completely unexpected finding was that D-LTCCs are essential for normal pacemaker activity in mouse heart. Reduced heart rate in $\alpha1D^{-/-}$ mice is compatible with the previous observation that voltage-gated Ca^{2+} channels, in addition to other ion channels (I_f "pacemaker" currents, acetylcholine-activated K^+ channels, the sustained inward current [I_{St}]; Wickman et al., 1998), control the spontaneous activity of the sinoatrial node. They contribute to diastolic depolarization (DiFrancesco, 1991; Guo et al., 1995; Verheijck et al., 1999) and mediate the upstroke of the action potential (Kodama et al., 1997). The contribution of LTCCs to diastolic depolarization has been considered to be minor because the activation threshold of LTCCs was found to be positive to −40 mV, whereas the pacemaker depolarization occurs between −60 and −40 mV (Irisawa et al., 1993; Hagiwara et al., 1988). However, our electrophysiological data in IHCs clearly indicate that mammalian D-LTCCs can activate at this more negative potential range (about −50 to −40 mV with 10 mM Ba^{2+}, Figure 3B; about −65 mV with 1.3 mM Ca^{2+}, Figure 3C). Thus, their voltage dependence of activation makes them more suitable pacemaker currents than L-type Ca^{2+} currents formed by α1C subunits that activate at more positive potentials (Hagiwara et al., 1988; Mikami et al., 1989). Our data also support the recent observation that in rabbit sinoatrial node, a small fraction of DHP-sensitive Ca^{2+} current is already activated at potentials as negative as −60 mV (Verheijck et al., 1999).

This role of D-LTCCs for cardiac pacemaker function is unexpected because C-LTCCs comprise the vast majority of DHP-sensitive LTCCs in mammalian heart (Safayhi et al., 1997; Takimoto et al., 1997) and D-LTCCs are even absent in ventricular cardiomyocytes (Takimoto et al., 1997). Recovery of normal electrical activity after atropine administration in $\alpha1D^{-/-}$ mice suggests that in the absence of parasympathetic tone, C-LTCCs provide sufficient Ca^{2+} inward current to allow normal action potential generation and propagation and must therefore coexist with D-LTCCs in sinoatrial node pacemaker cells. In the absence of D-LTCCs, parasympathetic tone would be expected to hyperpolarize atrial cells (due to activation of acetylcholine-activated K^+ channels; Wickman et al., 1998) and thereby move the membrane potential out of the range of activation of C-LTCCs. This explains why only the more negatively activating D-LTCCs

but not C-LTCCs can support normal cardiac pacemaking in the presence of parasympathetic tone.

Unlike for rabbit, experimental conditions for successful patch-clamp recordings from mouse sinoatrial node cells have not yet been established. Although we were therefore unable to determine the relative contribution of these two channel types for total L-type current like in IHCs, our finding that D-LTCC contribute to cardiac pacemaking has important therapeutic implications. As D-LTCCs are absent in heart ventricular muscle (Takimoto et al., 1997), they comprise an attractive target for novel bradycardic agents that lack negative inotropic effects for the treatment of congestive heart failure, myocardial ischemia, and sinus tachycardia of various origin. The absence of lethal arrhythmias in $\alpha 1D^{-/-}$ mice and the possibility of rapid functional antagonism of the drug effect by atropine treatment could comprise clinically relevant advantages over currently available nonselective LTCC blockers.

Experimental Procedures

Generation of $\alpha 1D^{-/-}$ Mice

Mouse genomic DNA clones (J14279Q4 and L2232Q3) encoding exon 2 of the α1D subunit were isolated from a LAWRIST7 129 mouse strain genomic library (RZPD Berlin). The targeting construct (Figure 1A) consisted of the thymidine kinase gene (*TK*), a 1.4 kb genomic fragment 5′ to exon 2, the neomycin resistance (*neo*) gene driven by the *pgk* promotor inserted in reverse direction into the ClaI site of exon 2, a 5 kb genomic fragment 3′ to exon 2, and the plamid pKO V910 (Lexicon Genetics). The *neo* cassette introduces multiple stop codons into all three reading frames of the α1D gene (Cacna1d). A total number of 672 transfected embryonic stem (ES) cell colonies (AB2.2, Lexicon Genetics) surviving after selection with G418 and FIAU were screened by Southern blot analysis with a 5′ external probe for clones with homologous recombination events. Out of 167 positive ES cell clones, two were selected for blastocyst injection to create chimaeric mice. Transmission of the mutant α1D allele from both clones was identified by the coat color and confirmed by Southern blot analysis. The positive F1 progeny was crossed with C57Bl/6J mice, and their F2 heterozygous offspring were interbred to generate homozygous knockouts ($\alpha 1D^{-/-}$) as well as heterozygous and wild-type littermates. α1D deficiency was further confirmed in immunoblot experiments. Brain microsomes (30 μg) were separated on 5% or 7% polyacryamide SDS–PAGE gels under reducing conditions, transferred to PVDF membranes, and probed with affinity-purified polyclonal anti-$\alpha 1D_{2121–2137}$ antibody (0.5 μg/ml) as described (Pichler et al., 1997). The antiserum was raised in rabbits against a synthetic peptide corresponding to an α1D-specific sequence (amino acid residues 2121–2137; Williams et al., 1992) and affinity purified as previously described (Striessnig et al., 1990).

Electrophysiological Recordings

IHCs of wild-type and $\alpha 1D^{-/-}$ mice were studied either in Cell-Tak-mounted, organotypic cochlear cultures at P3–P5 (Glowatzki et al., 1997) or following acute dissection of the organ of Corti (>P5). Organotypic cultures were used within 30 hr. For patch-clamp experiments, somata of IHC were exposed by removing the tectorial membrane and supporting cells with cleaning pipettes. A piece of the organ of Corti was mounted into a perfusion chamber and constantly superfused with extracellular solution composed of 142 mM NaCl, 0.7 mM NaH_2PO_4, 5.8 mM KCl, 1.3 mM $CaCl_2$, 0.9 mM $MgCl_2$, 5.6 mM D-glucose, and 10 mM HEPES (pH 7.4). Vitamins and amino acids for Eagle's minimal essential medium were added from concentrates (GIBCO–BRL). Currents were recorded in the whole-cell configuration using an AXOPATCH 200B amplifier at 20°C–22°C. Quartz glass pipettes with a resistance of 3–4.5 MΩ were used and filled with 120 mM CsOH•gluconic acid, 0.1 mM $CaCl_2$, 4 mM $MgCl_2$, 5 mM HEPES, 5 mM EGTA, 20 mM CsCl, 10 mM Na^+ phosphocreatine, 4 mM Na_2ATP, 0.3 mM GTP (pH 7.35), and 305 mosM (I1). To record Ba^{2+} currents, IHCs were locally perfused with a solution containing 10 mM $BaCl_2$, 159 mM Tris-(hydroxymethylamino)-methane•HCl, 5.6 mM glucose (pH 7.4), with/without DHP modulators. In some experiments, Ba^{2+} was exchanged for 10 mM Ca^{2+}; in this case the pipette solution contained Tris-(hydroxymethylamino)-methane as the main cation instead of Cs^+ to block all residual outward currents through K^+ channels (I2). To record Ca^{2+} currents in physiological solution (1.3 mM Ca^{2+}), a pipette solution containing 140 mM CsCl, 0.1 mM $CaCl_2$, 3 mM $MgCl_2$, 5 mM HEPES, 5 mM EGTA, and 3 mM Na_2ATP was used (I3). Series resistance compensation yielded values of Rs from 3–8 MΩ. Raw currents were corrected for linear leak currents, and potentials were corrected for the liquid junction potential (−13 mV or −4 mV for I1 and I3, respectively).

Measurement of Pacemaker Activity in Isolated Mouse Atria

Mice were sacrified by decapitation and exsanguination. The hearts were quickly removed from the animals and placed in Krebs-Henseleit solution (KHS, 118 mM NaCl, 4.7 mM KCl, 1.8 mM $CaCl_2$, 1.0 mM $MgCl_2$, 0.4 mM NaH_2PO_4, 19 mM $NaHCO_3$, and 5.5 mM glucose). The solution was gassed with 95% O_2–5% CO_2 and maintained at 37°C resulting in a pH of 7.4. The atria were separated from the ventricles and other tissues and vertically suspended in a 20 ml organ bath filled with KHS at 37°C. The free edge of the right atrium was anchored on the bottom of the organ bath, while the free edge of the left atrium was connected to an isometric force transducer (Battaglia-Rangoni TRB/200/2) coupled to a chart recorder (Battaglia-Rangoni KV 220). Each preparation was allowed to equilibrate for 60 min before pacemaker activity was recorded for 10 s every 15 min for 1 hr. Data obtained after 60–75 min were used for comparison of heart rates of wild-type and $\alpha 1D^{-/-}$ mice.

Auditory Brainstem Responses

Mice were anaesthetized with ketamine (100 mg/kg body weight) and auditory brainstem responses (ABRs) measured as described previously (Schrott et al., 1990). The animals were stimulated with 2000 broadband clicks of alternating polarity transmitted via insert earphones every 16.7 ms and ABRs recorded using percutaneous needle electrodes (mastoid negative, vertex positive), a physiological amplifier (amplification 70,000- to 150,000-fold, bandpass filter of 1 Hz to 3000 Hz) and a computer-controlled data acquisition system that performed averaging synchronized to stimulus onset. The stimulus intensity was increased in 10 dB steps from 10 dB SPL up to 70 dB SPL in wild-type and heterozygous or 120 dB SPL in $\alpha 1D^{-/-}$ mice. The minimum stimulation intensity required to elicit the typical ABR waveform was defined as hearing threshold.

Telemetric ECG Recordings

The telemetry system consisted of implantable transmitters (TA 10ETA-F20) measuring biopotentials and physical activity, the telemetry receivers (RA1010), and a consolidation matrix (BCM100) (DATA Science International) (Johansson and Thoren, 1997). After anesthesia with pentobarbital (70 mg/kg body weight), transmitters were implanted subcutaneously on the back of the mice. The negative lead was tunneled subcutaneously to the front side of the thorax and the positive lead to the xiphoid process. ECGs were recorded 3–8 days after the surgical procedure in unrestrained animals. Heart rate and activity counts were sampled overnight every three minutes. In addition, 30 s ECG recordings were sampled every 30 min with a sampling rate of 500 Hz. Resting or activity R–R intervals were calculated from representative overnight ECG recordings made during rest (0 activity counts) or high activity (>15 activity counts), respectively. In pharmacological experiments 30 s ECG recordings were obtained every 90 s 15 min before until 30 min after drug administration. Recordings obtained after a stable drug effect was observed were used for statistical analysis. QRS complex durations were calculated from lead I ECGs sampled with 2000 Hz from ketamine anaesthetized mice. For blockade of cardiac muscarinric and β-adrenergic receptors first atropine (1 mg/kg body weight) and after 15 min propranolol (20 mg/kg body weight) was administered i.p.

Measurement of Blood Glucose and Hormone Levels

Serum insulin levels were determined by using the Sensitive Rat Insulin RIA kit (LINCO, St. Charles, MO). Serum blood glucose levels

were measured using the Glucose (Trinder) Single Reagent System from Sigma (Vienna, Austria). Intraperitoneal glucose tolerance test was performed on 5- to 8-week-old mice fasted for more than 16 hr. Glucose (1.5 g/kg body weight) was injected into the intraperitoneal space, and blood samples were collected at different time points from the orbital sinus. Plasma catecholamine levels were determined as described earlier (Singewald and Philippu, 1993). Plasma thyroid hormone levels were determined by standard chemoluminescence immunoassay.

Statistics

All data are expressed as means ± SD (unless stated otherwise) for the indicated number of experiments. Student's t test was used to calculate the statistical significance of differences between two sets of averaged data.

Acknowledgments

We thank Dr. Greg Kaczorowski and Dr. Fabian F. Moebius for helpful comments on the manuscript, Dr. Nikolas Singewald for help with telemetric recordings and catecholamine determinations, Dr. Hermann Dietrich for advice with surgical procedures, Julia Meitz for expert technical assistance, Georg Wietzorrek for histological analysis of mouse hearts, Peter Schleich for help with ECG recordings, Dr. Maureen McEnery for an early bleed of an anti-α1D antibody, and Dr. Hartmut Glossmann for continuous support. This work was supported by grants from the FWF (P12641 to J. S.), the Österreichische Nationalbank (to J. S.), the Legerlotz-Foundation, and the DFG (EN 294/2-1,2 to J. E.).

Received March 6, 2000; revised April 24, 2000.

References

Ashcroft, F.M., and Rorsman, P. (1989). Electrophysiology of the pancreatic beta-cell. Prog. Biophys. Molec. Biol. *54,* 87–143.

Bech-Hansen, N.T., Naylor, M.J., Maybaum, T.A., Pearce, W.G., Koop, B., Fishman, G.A., Mets, M., Musarella, M.A., and Boycott, K.M. (1998). Loss-of-function mutations in a calcium-channel alpha1-subunit gene in Xp11.23 cause incomplete X-linked congenital stationary night blindness. Nat. Genet. *19,* 264–267.

Bohmer, A. (1988). The Preyer reflex—an easy estimate of hearing function in guinea pigs. Acta Otolaryngol. *106,* 368–372.

Boyer, C., Lehouelleur, J., and Sans, A. (1998). Potassium depolarization of mammalian vestibular sensory cells increases [Ca2+]i through voltage-sensitive calcium channels. Eur. J. Neurosci. *10,* 971–975.

Deisseroth, K., Heist, E.K., and Tsien, R.W. (1998). Translocation of calmodulin to the nucleus supports CREB phosphorylation in hippocampal neurons. Nature *392,* 198–202.

DiFrancesco, D. (1991). The contribution of the 'pacemaker' current (if) to generation of spontaneous activity in rabbit sino-atrial node myocytes. J. Physiol. (Lond.) *434*, 23–40.

Forrest, D., Erway, L.C., Ng, L., Altschuler, R., and Curran, T. (1996). Thyroid hormone receptor beta is essential for development of auditory function. Nat. Genet. *13,* 354–357.

Fuchs, P.A., Evans, M.G., and Murrow, B.W. (1990). Calcium currents in hair cells isolated from the cochlea of the chick. J. Physiol. (Lond.) *429*, 553–568.

Glowatzki, E., Ruppersberg, J.P., Zenner, H.P., and Rusch, A. (1997). Mechanically and ATP-induced currents of mouse outer hair cells are independent and differentially blocked by d-tubocurarine. Neuropharmacology *36,* 1269–1275.

Graef, I.A., Mermelstein, P.G., Stankunas, K., Neilson, J.R., Deisseroth, K., Tsien, R.W., and Crabtree, G.R. (1999). L-type calcium channels and GSK-3 regulate the activity of NF-ATc4 in hippocampal neurons. Nature *401,* 703–708.

Green, G.E., Khan, K.M., Beisel, D.W., Drescher, M.J., Hatfield, J.S., and Drescher, D.G. (1996). Calcium channel subunits in the mouse cochlea. J. Neurochem. *67,* 37–45.

Guo, J., Ono, K., and Noma, A. (1995). A sustained inward current activated at the diastolic potential range in rabbit sino-atrial node cells. J. Physiol. (Lond.) *483*, 1–13.

Hagiwara, N., Irisawa, H., and Kameyama, M. (1988). Contribution of two types of calcium currents to the pacemaker potentials of rabbit sino-atrial node cells. J. Physiol. (Lond.) *395*, 233–253.

Hardingham, G.E., Cruzalegui, F.H., Chawla, S., and Bading, H. (1998). Mechanisms controlling gene expression by nuclear calcium signals. Cell Calcium *23,* 131–134.

Hell, J.W., Westenbroek, R.W., Warner, C., Ahlijanian, M.K., Prystay, W., Gilbert, M.M., Snutch, T.P., and Catterall, W.A. (1993). Identification and differential subcellular localization of the neuronal class C and class D L-type calcium channel α1 subunits. J. Cell. Biol. *123,* 949–962.

Hudspeth, A.J., and Lewis, R.S. (1988). Kinetic analysis of voltage- and ion-dependent conductances in saccular hair cells of the bullfrog, Rana catesbeiana. J. Physiol. (Lond.) *400*, 237–274.

Irisawa, H., Brown, H.F., and Giles, W. (1993). Cardiac pacemaking in the sinoatrial node. Physiol. Rev. *73,* 197–227.

Ison, J.R., Payman, G.H., Palmer, M.J., and Walton, J.P. (1997). Nimodipine at a dose that slows ABR latencies does not protect the ear against noise. Hear. Res. *106,* 179–183.

Iwashima, Y., Pugh, W., Depaoli, A.M., Takeda, J., Seino, S., Bell, G.I., and Polonsky, K.S. (1993). Expression of calcium channel mRNAs in rat pancreatic islets and downregulation after glucose infusion. Diabetes *42,* 948–955.

Johansson, C., and Thoren, P. (1997). The effects of triiodothyronine (T3) on heart rate, temperature and ECG measured with telemetry in freely moving mice. Acta Physiol. Scand. *160,* 133–138.

Jumrussirikul, P., Dinerman, J., Dawson, T.M., Dawson, V.L., Ekelund, U., Georgakopoulos, D., Schramm, L.P., Calkins, H., Snyder, S.H., Hare, J.M., and Berger, R.D. (1998). Interaction between neuronal nitric oxide synthase and inhibitory G protein activity in heart rate regulation in conscious mice. J. Clin. Invest. *102,* 1279–1285.

Kodama, I., Nikmaram, M.R., Boyett, M.R., Suzuki, R., Honjo, H., and Owen, J.M. (1997). Regional differences in the role of the Ca2+ and Na+ currents in pacemaker activity in the sinoatrial node. Am. J. Physiol. *272,* H2793–H2806.

Kollmar, R., Montgomery, L.G., Fak, J., Henry, L.J., and Hudspeth, A.J. (1997). Predominance of the alpha1D subunit in L-type voltage-gated Ca2+ channels of hair cells in the chicken's cochlea. Proc. Natl. Acad. Sci. USA *94,* 14883–14888.

Liberman, M.C., and Dodds, L.W. (1984). Single-neuron labeling and chronic cochlear pathology. III. Stereocilia damage and alterations of threshold tuning curves. Hear. Res. *16,* 55–74.

Lopez, I., Ishiyama, G., Ishiyama, A., Jen, J.C., Liu, F., and Baloh, R.W. (1999). Differential subcellular immunolocalization of voltage-gated calcium channel alpha1 subunits in the chinchilla cristae ampullaris. Neuroscience *92,* 773–782.

Martinez-Dunst, C., Michaels, R.L., and Fuchs, P.A. (1997). Release sites and calcium channels in hair cells of the chick's cochlea. J. Neurosci. *17,* 9133–9144.

Mikami, A., Imoto, K., Tanabe, T., Niidome, T., Mori, Y., Takeshima, H., Narumiya, S., and Numa, S. (1989). Primary structure and functional expression of the cardiac dihydropyridine-sensitive calcium channel. Nature *340,* 230–233.

Moser, T., and Beutner, D. (2000). Kinetics of exocytosis and endocytosis at the cochlear inner hair cell afferent synapse of the mouse. Proc. Natl. Acad. Sci. USA *97,* 883–888.

Murphy, T.H., Worley, P.F., and Baraban, J.M. (1991). L-type voltage-sensitive calcium channels mediate synaptic activation of immediate early genes. Neuron *7,* 625–635.

Pichler, M., Cassidy, T.N., Reimer, D., Haase, H., Kraus, R., Ostler, D., and Striessnig, J. (1997). Beta subunit heterogeneity in neuronal L-type calcium channels. J. Biol. Chem. *272,* 13877–13882.

Rajadhyaksha, A., Barczak, A., Macias, W., Leveque, J.C., Lewis, S.E., and Konradi, C. (1999). L-Type Ca(2+) channels are essential for glutamate-mediated CREB phosphorylation and c-fos gene expression in striatal neurons. J. Neurosci. *19,* 6348–6359.

Safayhi, H., Haase, H., Kramer, U., Bihlmayer, A., Roenfeldt, M.,

Ammon, H.P., Froschmayr, M., Cassidy, T.N., Morano, I., Ahlijanian, M., and Striessnig, J. (1997). L-type calcium channels in insulin-secreting cells: biochemical characterization and phosphorylation in RINm5F cells. Mol. Endocrinol. *11,* 619–629.

Schrott, A., Stephan, K., and Spoendlin, H. (1990). Auditory brainstem response thresholds in a mouse mutant with selective outer hair cell loss. Eur. Arch. Otorhinolaryngol. *247,* 8–11.

Singewald, N., and Philippu, A. (1993). Catecholamine release in the locus coeruleus is modified by experimentally induced changes in haemodynamics. Naunyn Schmiedebergs Arch. Pharmacol. *347,* 21–27.

Striessnig, J. (1999). Pharmacology, structure and function of cardiac L-type Ca(2+) channels. Cell. Physiol. Biochem. *9,* 242–269.

Striessnig, J., Glossmann, H., and Catterall, W.A. (1990). Identification of a phenylalkylamine binding region within the alpha1 subunit of skeletal muscle Ca2+ channels. Proc. Natl. Acad. Sci. USA. *87,* 9108–9112.

Strom, T.M., Nyakatura, G., Apfelstedt-Sylla, E., Hellebrand, H., Lorenz, B., Weber, B.H., Wutz, K., Gutwillinger, N., Ruther, K., et al. (1998). An L-type calcium-channel gene mutated in incomplete X-linked congenital stationary night blindness. Nat. Genet. *19,* 260–263.

Takimoto, K., Li, D., Nerbonne, J.M., and Levitan, E.S. (1997). Distribution, splicing and glucocorticoid-induced expression of cardiac alpha 1C and alpha 1D voltage-gated Ca2+ channel mRNAs. J. Mol. Cell. Cardiol. *29,* 3035–3042.

Tao, X., Finkbeiner, S., Arnold, D.B., Shaywitz, A.J., and Greenberg, M.E. (1998). Ca2+ influx regulates BDNF transcription by a CREB family transcription factor-dependent mechanism. Neuron *20*, 709–726. Erratum: Neuron *20* (6), 1297, 1998.

Verheijck, E.E., van Ginneken, A.C., Wilders, R., and Bouman, L.N. (1999). Contribution of L-type Ca2+ current to electrical activity in sinoatrial nodal myocytes of rabbits. Am. J. Physiol. *276,* H1064–H1077.

Wickman, K., Nemec, J., Gendler, S.J., and Clapham, D.E. (1998). Abnormal heart rate regulation in GIRK4 knockout mice. Neuron *20,* 103–114.

Williams, M.E., Feldman, D.H., McCue, A.F., Brenner, R., Velicelebi, G., Ellis, S.B., and Harpold, M.M. (1992). Structure and functional expression of alpha1, alpha2, and beta subunits of a novel human neuronal calcium channel subtype. Neuron *8,* 71–84.

Yamada, Y., Masuda, K., Li, Q., Ihara, Y., Kubota, A., Miura, T., Nakamura, K., Fujii, Y., Seino, S., and Seino, Y. (1995). The structures of the human calcium channel α_1 subunit (CACNL1A2) and β subunit (CACNLB3) genes. Genomics *27,* 312–319.

Zheng, Q.Y., Johnson, K.R., and Erway, L.C. (1999). Assessment of hearing in 80 inbred strains of mice by ABR threshold analyses. Hear. Res. *130,* 94–107.

Zidanic, M., and Fuchs, P.A. (1995). Kinetic analysis of barium currents in chick cochlear hair cells. Biophys. J. *68,* 1323–1336.